

Full-Wave Electromagnetic Model Simulations of *P*-Band Radio Signal Propagation Through Forest Using the Fast Hybrid Method

Jongwoo Jeong¹, Graduate Student Member, IEEE, Leung Tsang², Life Fellow, IEEE, Xiaolan Xu¹, Member, IEEE, Simon H. Yueh, Fellow, IEEE, and Steven A. Margulis¹

Abstract—This article presents an analysis of *P*-band radio signal propagation through forest based on 3D Numerical Method of Maxwell's equations (NMM3D). The simulation domain of the forested region covers an area of $35.8 \times 35.8 \text{ m}^2$ that includes 112–121 coniferous trees with a height in the range of 8–16 m. The modeled trees have primary and secondary branches to account for their impact on scattering and attenuation at *P*-band. The fast hybrid method (FHM) has been successfully developed to complete the NMM3D full wave simulations of trees with efficient use of CPU time and memory. The accuracy of the proposed FHM model is validated by comparing scattered fields to that of FEKO for the case with nine trees. To account for the seasonal variation of water content in trees and hence dielectric constant, the wave scattering model is applied to a range of dielectric constants. Analysis of the *P*-band signal propagation is performed by computing the average loss and correlation of the transmission fields. The results show that the transmissivities are about 0.9 for winter conditions (low dielectric constant) and about 0.7 for summer conditions (high dielectric constant). Simulations with randomly positioned trees (off the periodic grid) demonstrate that the transmissivity shows a maximum variation of 4.3% relative to the nonrandomly positioned trees. The correlation analysis of *P*-band radio signals with two different dielectric constants indicates a high correlation amplitude above 0.89 and a phase change of less than 6° . A sensitivity analysis is carried out for a range of tree heights and trunk radii.

Index Terms—Electromagnetic modeling, electromagnetic scattering, full-wave simulations, hybrid method, Maxwell equations 3-D, random media, remote sensing.

I. INTRODUCTION

P-BAND radio signals have long been of great interest in radar remote sensing since they have high penetration through dense forest canopies. With the use of *P*-band signals,

Manuscript received 18 March 2023; revised 16 May 2023; accepted 24 June 2023. Date of publication 5 July 2023; date of current version 27 July 2023. This work was supported by the NASA Remote Sensing Theory Program. (Corresponding author: Jongwoo Jeong.)

Jongwoo Jeong and Leung Tsang are with the Department of Electrical Engineering and Computer Science, University of Michigan, Ann Arbor, MI 48105 USA (e-mail: jjongwoo@umich.edu; leutsang@umich.edu).

Xiaolan Xu and Simon H. Yueh are with the Jet Propulsion Laboratory, California Institute of Technology, Pasadena, CA 91109 USA (e-mail: xiaolan.xu@jpl.nasa.gov; simon.h.yueh@jpl.nasa.gov).

Steven A. Margulis is with the Department of Civil and Environmental Engineering, University of California, Los Angeles, CA 90095 USA (e-mail: margulis@seas.ucla.edu).

Digital Object Identifier 10.1109/JSTARS.2023.3292324

various data such as soil moisture, land topography, and snow can be extracted with less influence by forests [1], [2]. Despite its hypothesized advantage, *P*-band signal propagation through forest has not been rigorously analyzed before. Considering the fact that dielectric constant of trees varies seasonally [3], it is necessary to analyze *P*-band signal propagation through trees with respect to different dielectric constants.

For several decades, the radiative transfer equation (RTE)/distorted Born approximation has been used to model the scattering of electromagnetic waves by forest [4], [5]. For the modeling of forest scattering, RTE represents trees as a collection of cylinders (trunks, branches, and needle leaves) and thin disks (leaves), which are homogeneous and randomly distributed in the forest. This leads to a simplified scattering model, which can be implemented by considering independent scattering from all vegetation elements. These approximations for the RTE have never been rigorously tested. Comparisons with the exact numerical solutions of Maxwell's equations indicate that the accuracy of RTE is limited [9], [17].

RTE [20] is not a rigorous approach based on assumptions that are not fully justified, in particular the completely independent random positions of trees. In addition, using intensities rather than complex field amplitudes does not allow for the complex correlation analysis to study the impact of tree dielectric constant on decorrelation of transmission fields. The fast hybrid method (FHM) is a rigorous way of solving wave multiple scattering and gives exact solutions of Maxwell's equations. Microwaves in trees are governed exactly by Maxwell's equations and not by RTE.

In [6], the infinite cylinder approximation, including multiple scattering, has been applied to forests at the UHF band. However, this model is limited to trunk-dominated forest for applications in wireless communications. Unlike the analysis of propagation of lateral waves in [6], *P*-band microwave signals for radar remote sensing are transmitted by satellites above the forest canopies, and therefore our interests are the propagation of the signals from above and through canopies for the imaging of the soil or snow beneath the forests.

To accurately model the *P*-band signal propagation through forest canopies, gaps between trees, heights of trees, and realistic 3-D representation of trees should be incorporated into an electromagnetic scattering model. Our approach is rigorous by using

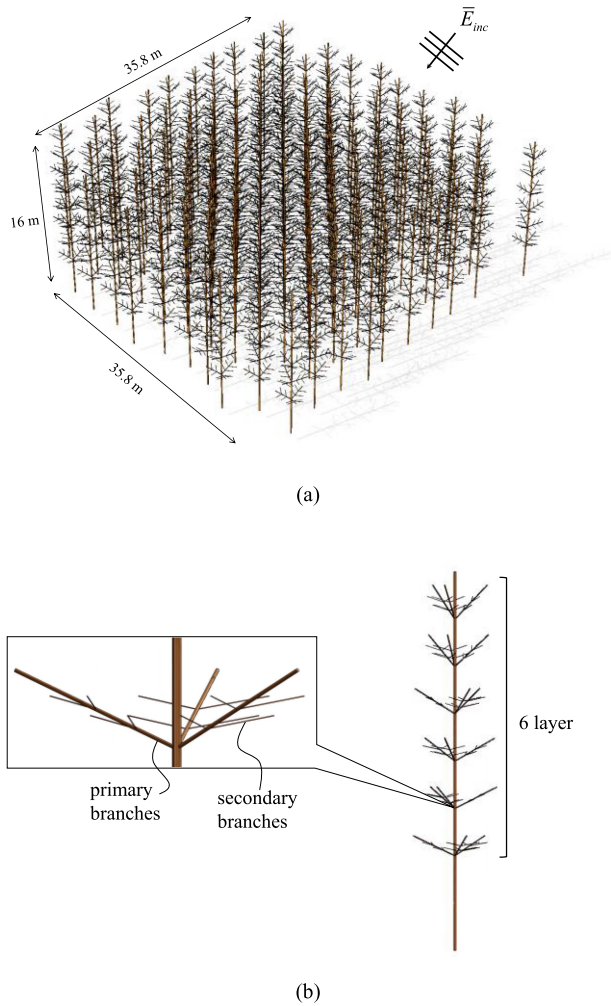


Fig. 1. Geometric configuration of (a) forest of coniferous trees occupying a space of $35.8 \times 35.8 \text{ m}^2$ and (b) the shapes of a single tree.

the 3-D full-wave simulations of microwave scattering based on Maxwell's equations. Among various full-wave simulation solvers available through commercial vendors, those methods that have been widely used include: finite-element method used by HFSS, method of moments used by FEKO, and the finite-difference time-domain used by CST [7], [13]. However, for the conditions in a realistic forest plot (e.g., Fig. 1 with a coniferous tree height of 16 m and more than 100 trees), full-wave simulations using commercial software are not yet computationally practical (in terms of both CPU time and memory).

For efficient simulations of microwave propagation through forest, a hybrid method was proposed in [8] and [9]. It is based on numerical solutions for extracting scattering characteristics of a single tree and analytical solutions for calculating multiple scattering based on vector cylindrical waves (VCWs). The hybrid method is performed using a two-step approach. The first step is to extract the T-matrix representing wave scattering for a single tree using the accurate commercial software. The second step is to compute multiple wave scattering among trees based on the Foldy-Lax equation. In the second step, since the T-matrix is

reused and it calculates electromagnetic interactions only outside of enclosing cylinders, the hybrid method can significantly reduce CPU time and memory for full-wave simulations. In [8], the hybrid method was successfully applied to 196 trees using an infinite cylinder approximation. Due to the height of trees in scattering simulations, a large number of unknowns are generated to calculate multiple scattering, which leads the hybrid method being reliant on high-performance computing (HPC). The P -band signal propagation and scattering analysis for forests require a large number of simulations to account for a range of dielectric constant and the geometric parameters of trees. As a result, it is necessary to employ fast solutions to model electromagnetic scattering of a forest layer. Therefore, the FHM, to speed up multiple scattering solutions, is adopted for P -band radio signals.

Previously, the hybrid method with fast Foldy-Lax matrix inversion solutions and an iterative approach, was applied to 30 trees at L -band [9]. However, the computational complexity arising from the matrix-column vector multiplication with the Foldy-Lax matrix remains unaddressed. To further reduce CPU time and memory requirements, FHM was developed for wave propagation through corn plants [10]. In the FHM, the solution of Foldy-Lax equations is accelerated by a triple FFT. Two orders of the FFTs are based on the sparse matrix canonical grid method (SMCG) in 2-D positions of the trees [11]. The third order of the FFTs is based on the order of the VCW. The FHM was shown to simulate radio signals through 100 corn plants in less than 6 min using a standard laptop computer [10].

The water content of trees varies due to water availability in the soil and influences dielectric constant variation [3]. Thus, it is important to analyze P -band radio signals for a range of dielectric constants. Based on these parameters, we can assess forest effects and sensitivity of the P -band radio signal propagation to the seasonal change of forests.

In this article, we analyze P -band signal propagation through forests by using the electromagnetic scattering model of the FHM. This article is organized as follows. First, the P -band signal propagation through forest requires an estimate of an adequate number of trees within the domain of simulation. Following that, the scattering model of the FHM is described. After that, the scattering model is applied to 121 trees with heights of 8, 12, and 16 m and diameters in the range of 10–30 cm. Because the dependence is monotonic, parametric models can be generated by the FHM for trees with various heights and radii. To cover various tree configuration scenarios, the randomly positioned trees and mixed trees are considered in the FHM. A case study is completed to illustrate the relative transmissivity at P -band and L -band, with the aim of showing the higher penetration at lower frequencies.

II. METHOD FOR SIMULATION OF P -BAND SIGNAL

In order to analyze P -band signals, modeling of wave scattering is formed by the electromagnetic response of tree objects to the incident plane wave. Specifically, the impingement of plane incident waves on multiple trees is simulated, and the scattered waves from these trees are computed by the FHM.

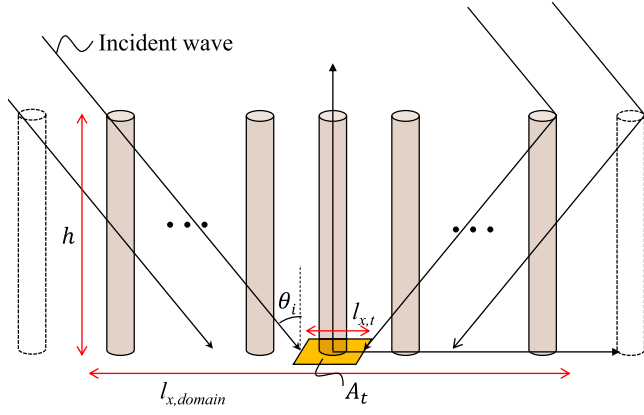


Fig. 2. Estimation of the number of trees for the wave scattering model.

For further characterization of forest effects on P -band signals, we focus on the center area of the forest for average transmit power calculation to avoid edge effects. Due to the limited spatial domain, some of the trees are located on the edge of forest, and the transmitted power under them should not be used for averaging. This central area is defined as A_t , an area for calculating transmitted power. By increasing the size of A_t , we can take the average of the transmitted power with respect to the area. A_t can be used to determine the number of trees needed in wave scattering modeling.

A. Estimation of the Number of Trees

A crucial part in the simulation of scattering of the P -band signal is the estimation of the required size of domain and hence the number of trees. For our scattering model, the spatial distribution of trees is illustrated in Fig. 2. We require A_t to be large enough so that there will be a large number of trees to allow convergence to a representative solution, but not too large to avoid edge effects. Note that if A_t is too large, incident waves will have experienced only partial attenuation and scattering by some trees near the edge of A_t , resulting in a higher (erroneous) transmission. In simulation results, we have two areas: 1) A_{domain} , which is the domain of the simulation and 2) A_t , which is the domain over which we calculate the scattered fields and transmitted fields. Plane wave incidence is assumed on A_{domain} . To avoid edge effects, A_t must be less than A_{domain} . For convergence validation, we need to increase A_t under the fixed A_{domain} obtained by the design formula. This approach is different from traditional approaches of rough surface simulations in which a tapered wave is used. However, a tapered wave approach is poor when the height is larger or much larger than a wavelength. By considering the tree height h (see Fig. 2), the domain width is described as

$$l_{x,\text{domain}} = 2h \tan \theta + l_{x,t} \quad (1)$$

where θ_i and $l_{x,t}$ are an incident angle and a side length of A_t , respectively. Once $l_{x,t}$ is determined, the width of the domain area is calculated by (1).

TABLE I
DIMENSIONS OF A TRUNK AND BRANCHES

	Trunk	Primary branch	Secondary branch
Number	1	18	72
Length [m]	16	1.6	0.8
Radius [cm]	5	2	0.5

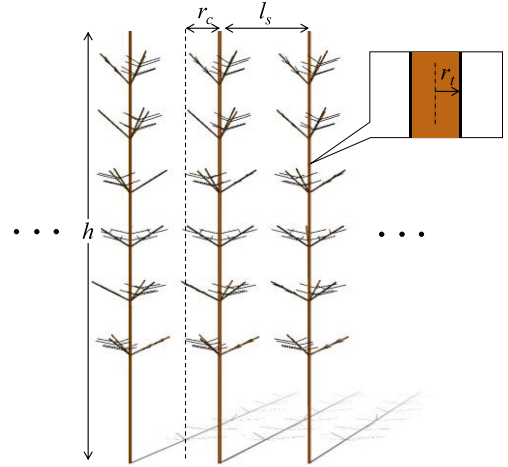


Fig. 3. Parameters of tree dimensions and their locations.

Table I shows the values of the tree dimensions shown in Fig. 3. The variable r_t indicates the radius of the trunk to be used in parametric models. The tree branches are distributed into six layers with 2 m spacing between them. Each layer contains three primary branches and 12 secondary branches. The layers of branches are arranged in an asymmetric pattern by rotating them along azimuthal angles. When we consider a tree height of 16 m, the incidence angle θ_i of 40° , and $l_{x,t} = 9$ m, the width of the simulation domain is 35.8 m. Considering a spacing l_s between trees of 3.3 m and r_c of 1.4 m, we determine that the number of trees in the domain area is 121 trees.

Scattering simulations over the study domain, containing 121 trees with a 16 m height require substantial computation resources. For the efficient computation and fast simulations of a large number of trees, the FHM is employed to model the wave scattering [10].

B. Fast Hybrid Method

The first step of the FHM is to extract the T-matrix of a single tree. To efficiently solve the scattered fields of a large number of trees, treating a single tree as a single network parameter, the T-matrix [18], can reduce the unknowns in Maxwell's equations and the computational complexity. The T-matrix characterizes the scattered field coefficients in terms of VCW as follows [9], [12]:

$$a_n^{S\alpha}(k_z) = \sum_{\beta \in \{M, N\}} \sum_{n'} \int_{-k}^k dk'_z T_{nn'}^{(\alpha, \beta)}(k_z, k'_z) a_{n'}^{E\beta}(k'_z), \quad \alpha = M, N \quad (2)$$

where $a_{n'}^{E\beta}(k'_z)$ is the complex amplitude of excitation field, α and β are VCW modes corresponding to \bar{M} or \bar{N} used in electric field calculation as shown in the following equation:

$$\bar{E}^s(\bar{r}) = \sum_n \int_{-k}^k dk_z \left[a_n^{SM}(k_z) \bar{M}_n(k_z, \bar{r}) + a_n^{SM} \bar{N}_n(k_z, \bar{r}) \right].$$

$T_{nn'}^{(\alpha,\beta)}(k_z, k'_z)$ in (2) is a T-matrix element corresponding to a cylindrical wave order of n and a z -directional component of the wave vector k_z . Scattered fields are calculated based on coefficients of VCWs. When considering P -band signals, to only consider propagating waves requires restricting the k_z wave modes to a maximum wave number of k . This is necessary as the wave numbers past this limit correspond to evanescent waves and thus have a negligible contribution. Using full-wave solvers such as FEKO and HFSS, we can excite plane waves and store scattering amplitudes from a single tree. Far-field solutions of VCW are matched with full-wave solutions of commercial software, and this provides the calculation of T-matrix elements as discussed in [12].

The second step is to solve multiple scattering among trees based on the Foldy–Lax equation. The Foldy–Lax equation states that the final excitation fields are equivalent to the sum of incident waves and scattered waves

$$\bar{E}_q^{ex}(\bar{r}) = \bar{E}^{inc}(\bar{r}) + \sum_{p=1, p \neq q}^N \bar{E}_{qp}^s(\bar{r}) \quad (3)$$

where p and q are indices of scatterers and summation is performed except $p \neq q$. With the aid of a matrix form of (3) [10], we can formulate it as a system of linear equations

$$\begin{pmatrix} \psi_{inc}^M \\ \psi_{inc}^N \end{pmatrix} = \begin{pmatrix} \mathbf{I} - \mathbf{F}^{MM} & -\mathbf{F}^{MN} \\ -\mathbf{F}^{NM} & \mathbf{I} - \mathbf{F}^{NN} \end{pmatrix} \begin{pmatrix} \mathbf{a}^{SM} \\ \mathbf{a}^{SN} \end{pmatrix} \quad (4)$$

where

$$\begin{aligned} & F_{qm',pn}^{\beta,\alpha}(k_{z,n_z}, k'_{z,n_z}) \\ &= \sum_m T_{m'm}^{(\beta,\alpha),q}(k_{z,n_z}, k'_{z,n_z}) \sigma_{mn}^{qp}(k'_{z,n_z}) \\ & \sigma_{mn}^{qp}(k_{z,n_z}) \\ &= \begin{cases} \Delta k_z H_{m-n}^{(1)}(k_{\rho,n_z} |\bar{\rho}_p - \bar{\rho}_q|) e^{-i(m-n)\phi_{\bar{\rho}_p \bar{\rho}_q}} \\ \times e^{-ik_{z,n_z}(z_p - z_q)}, \text{ for } q \neq p \\ 0, \text{ for } q = p \end{cases} \\ & \psi_{qm'}^{inc,\beta}(k_{z,n_z}) = \sum_m \exp(i\bar{k}_i \cdot \bar{r}_q) \frac{i^m \exp(-im\phi_i)}{k_{ip}} \\ & \times \left[iE_{hi} T_{m'm,q}^{(\beta,M)}(k_{z,n_z}, k_{iz}) - E_{vi} T_{m'm,q}^{(\beta,N)}(k_{z,n_z}, k_{iz}) \right] \end{aligned}$$

k_{z,n_z} is discretization over k_z range with spacing Δk_z and $\sigma_{mn}^{qp}(k_{z,n_z})$ is a translation addition matrix. The matrix dimension of block matrices, \mathbf{F} and \mathbf{I} , is $N_q N_m N_n \times N_q N_m N_n$, where N_q , N_m , and N_n represent the number of trees, of azimuthal mode, and of discretized k_z , respectively. The plane wave coefficients are $E_{vi} = -iE_R/\sqrt{2}$ and $E_{hi} = E_R/\sqrt{2}$ to generate the right-hand circular polarization (RHCP).

Since the matrix multiplication in (4) increases computational complexity as the number of trees grows, the third step is introduced to speed up the solutions of the Foldy–Lax matrix equations. Considering trees periodically located on the x – y plane, the locations of trees are represented by indices as

$$\bar{\rho}_p = \hat{x}\alpha'_g \Delta x + \hat{y}\beta'_g \Delta y \quad (5)$$

where α'_g and β'_g are corresponding to tree locations with their ranges $\alpha'_g \in [1, N_x]$ and $\beta'_g \in [1, N_y]$, respectively. N_x and N_y are the number of trees along x -axis and y -axis, respectively. This notation leads to the formulation of the triple FFT consisting of 2-D FFTs for spatial distribution of trees on the x – y plane and 1-D FFT for the order of cylindrical waves in translation addition theorem. The triple FFT is applied to the translation addition matrix and a column vector as shown in the following equation [15]:

$$\begin{aligned} \sigma_F &= \text{FFT} \{ \sigma \} \\ \mathbf{a}_F^{S\alpha} &= \text{FFT} \{ \mathbf{a}^{S\alpha} \} \end{aligned} \quad (6)$$

where both σ_F and $\mathbf{a}_F^{S\alpha}$ have the three dimensions of $2N_x \times 2N_y \times (4N_{\max} + 2)$. The inverse triple FFT of (6) provides a matrix multiplication by a column vector as shown in the following equation:

$$\psi^\alpha = \text{FFT}^{-1} \{ \sigma_F \circ \mathbf{a}_F^{S\alpha} \}. \quad (7)$$

Due to the large number of unknowns, the inversion of the matrix increases CPU time and memory in the hybrid method. To calculate unknowns in (4), the inversion of the Foldy–Lax matrix is transformed into physical iterative solutions [9], [16]. This means that the iterative multiplication of the Foldy–Lax matrix provides the n th-order solutions, where n is the number of iterations. The higher order solutions converge rapidly.

Since scattering coefficients are defined outside the cylinder that encloses a tree, plane waves are used to compute the inner field in the commercial software [10].

C. Validation: FHM and Estimated Number of Trees

For validation of our hybrid method, the specification of incident waves is based on the P -band Signals of Opportunity Synthetic Aperture Radar concept [2]. The frequency is 370 MHz, and polar and azimuthal angles of plane incident waves are $\theta_i = 40^\circ$ as shown in Fig. 2 and $\phi_i = 0^\circ$, respectively. The coefficient of RHCP waves is $E_R = 1$. The entire procedure for FHM is shown in Fig. 4. During preprocessing, the T-matrix is computed and stored in the library. Using Altair FEKO [13], the scattered fields of a single tree are computed, and the T-matrix extraction formula in (4) characterizes the T-matrix. The complex permittivity of the trees determined by the dielectric model in [14] ranges from $3 + 0.70i$ to $20 + 10.07i$. The extracted T-matrices corresponding to dielectric constants are validated by comparing scattered fields of FHM to that of FEKO, as shown in Fig. 5(b). The complex permittivity of the tree is used for simulation, but for the sake of brevity, only the real part, ϵ'_r , is used to label the curves in the figures throughout this article. The field points are $1.4 \leq x \leq 15$ m, $y = 0$ m, $z = 0$ m, as shown in Fig. 5(a).

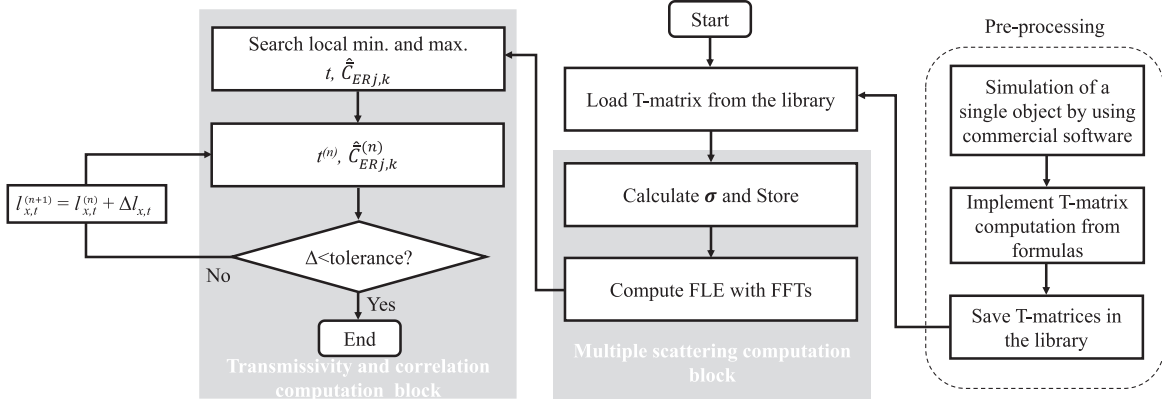


Fig. 4. FHM procedure for computing transmissivity and correlation coefficients. In the transmissivity and correlation computation block, t , the index n , and $\Delta I_{x,t}$ are a transmissivity, the number of the iteration, and an increase of $I_{x,t}$, respectively.

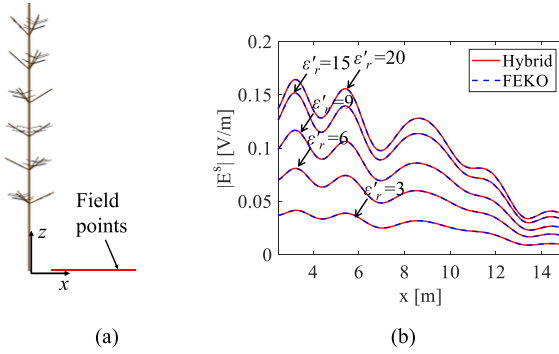


Fig. 5. Validation of T-matrices corresponding to different dielectric constants. (a) Field points for validation. (b) Comparison of scattered fields obtained using T-matrix and FEKO.

Following T-matrix extraction, the second step, calculating multiple scattering, is validated by the commercial software FEKO. With the configuration of 3×3 trees and the tree parameters of $\epsilon'_r = 6$, $h = 16$ m, and $l_s = 3.3$ m as shown in Fig. 6(a), the accuracy of the wave scattering model from FHM is compared to FEKO. To check iterative solutions for the matrix, scattering coefficients corresponding to the first tree's \bar{M} modes are plotted in Fig. 6(b). For visualization, the points in Fig. 6 are sampled every 20 indices. This indicates that higher order solutions decrease quickly as the orders increase. Therefore, including up to the second order is sufficient to accurately capture multiple scattering. As shown in Fig. 6(c), the scattered fields of the FHM are plotted at observed points along the x -direction ($-15 \leq x \leq 15$ m, $y = 1.6$ m, $z = 0$ m) and y -direction ($x = 1.6$ m, $-15 \leq y \leq 15$ m, $z = 0$ m), which show good agreement with FEKO. Our primary interests are the characteristics of P -band signals on the ground plane beneath the forest, and thus the electric and magnetic fields of the FHM on the x - y plane at $z = 0$ m are compared to that of FEKO as shown in Fig. 6(d), which show excellent agreement.

The FHM reduces computational complexity and memory requirements. For P -band signal propagation through a forest,

TABLE II
CPU TIME AND MEMORY COMPARISON

	FEKO	FHM (FEKO combined w. Foldy–Lax Equation)
CPU time (s)	263.6	192.8
Memory (GB)	111.45	0.53
Computing resource	High performance computer	Standard laptop

hybrid solutions that combine FEKO with analytical solutions of the Foldy–Lax equation provide more efficient and faster solutions than solely simulating the forest using FEKO. For the CPU time and memory comparison, the FHM was performed using Ryzen 5 4500U (standard laptop) and 16 GB RAM, whereas FEKO simulation was performed by Intel Xeon Gold 6254 CPU with 180 GB RAM (HPC). The comparison is described in Table II. The CPU time of the FHM is 27% less than that of FEKO and the memory usage is 210 times less than FEKO. Note that the difference of CPU time and memory between the FHM and FEKO becomes large as the number of trees increases. Due to its relatively small memory capacity, the FHM is capable of modeling wave scattering of P -band signals over much larger domains than commercial software, which exceeds its memory limit. For this reason, we chose to apply the FHM in our study.

In order to validate the proposed number of trees, we design the test case that compares transmissivity between nine trees by using FEKO and 121 trees by the FHM. Transmissivity is the ratio between transmitted power reaching through trees and incident power as shown in the following equation:

$$T = \frac{1}{A_t} \iint_{A_t} \frac{\bar{S}^{tot} \cdot (-\hat{z})}{\bar{S}^{inc} \cdot (-\hat{z})} d\bar{r} \quad (8)$$

where \bar{S}^{tot} is Poynting vectors obtained from total electric fields and total magnetic fields, and \bar{S}^{inc} is Poynting vector of incident fields. Transmissivity computation involves two regions, as shown in Fig. 7: A_t , which is used for calculating transmitted power, and A_d , which is the domain area where all the trees are located. Incident waves reach A_d as shown in Fig. 7, and the FHM computes multiple scattering in this area. The transmissivity is computed over A_t . Since the transmissivity fluctuates depending

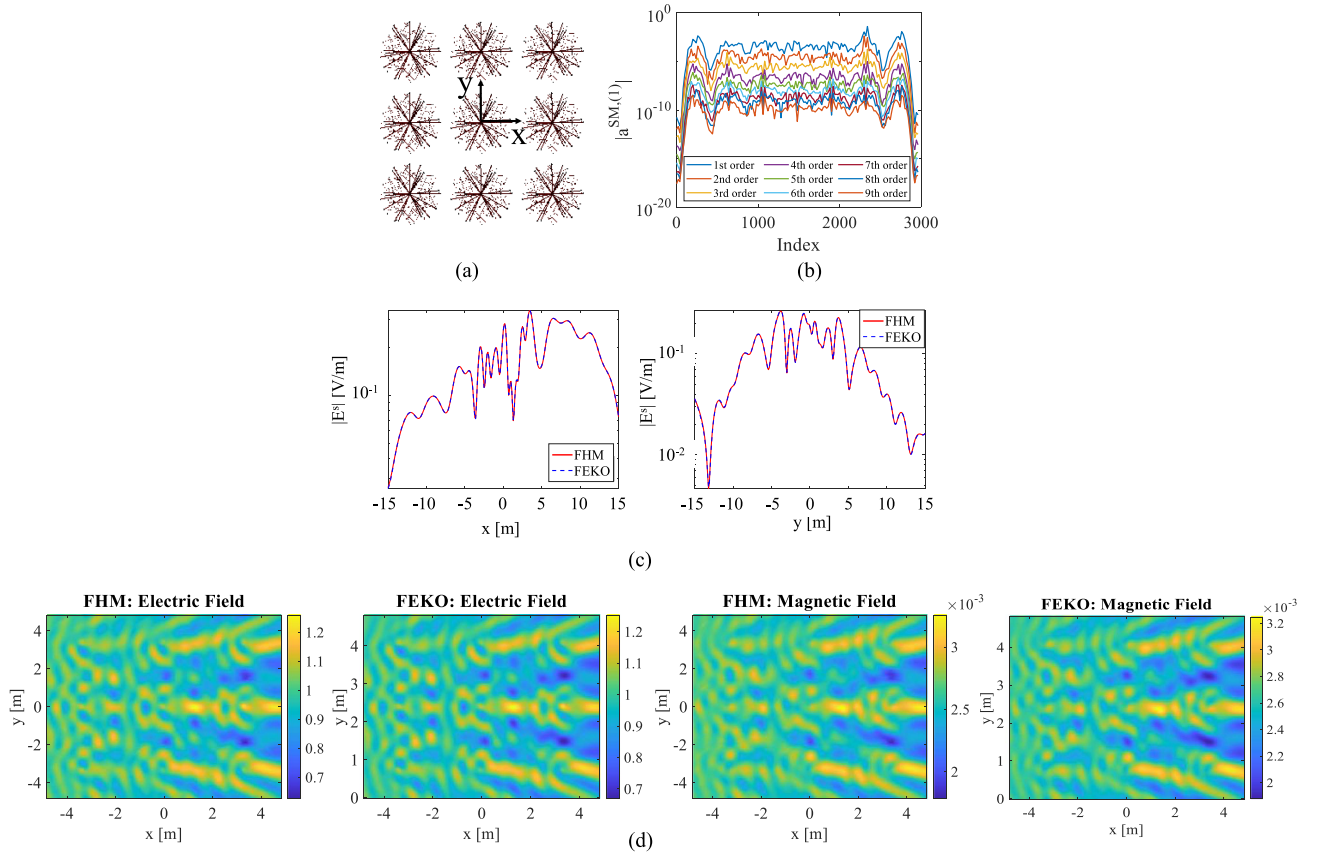


Fig. 6. Validation of the scattering model using nine trees. (a) Top view of nine-tree arrangement. (b) Rapidly decreasing scattering wave coefficients with an increasing order in physical iterative solutions. (c) Comparison of scattered fields between the FHM and FEKO. (d) P -band signals on the bottom plane.

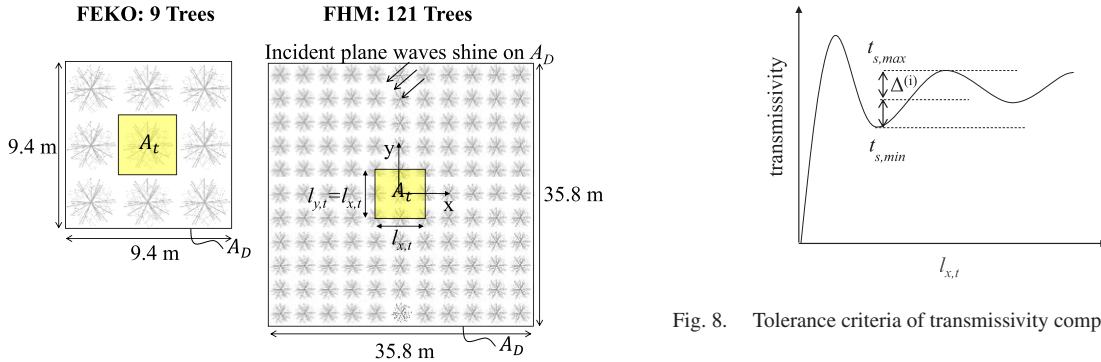


Fig. 7. Definition of A_D and A_t , and the test case of 9 trees and 121 trees.

on the size of A_t , it is necessary to find convergent values by increasing A_t . The transmissivity computation block in the FHM process is described in Fig. 4. After searching a zero slope to find local minimum and maximum values, transmissivity is iterated by increasing the side length $l_{x,t}$ in Fig. 7. The transmissivity is obtained by taking the center point between local minimum and maximum values. Then, it is completed when it satisfies the following:

$$\frac{2\Delta}{t_{s,\max} + t_{s,\min}} < \text{tolerance} \quad (9)$$

Fig. 8. Tolerance criteria of transmissivity computation.

TABLE III
TRANSMITTED POWER COMPARISON

	FEKO	FHM
Number of trees	9	121
Transmissivity	0.968	0.891

The bold values indicate the value of the FHM.

where variables are defined in Fig. 8. The transmissivity results by using the test case are shown in Table III. To show edge effects and validate the selected number of trees, we compare the transmissivity between 9 and 121 trees. In the nine-tree case, some incident waves reach A_t without passing through

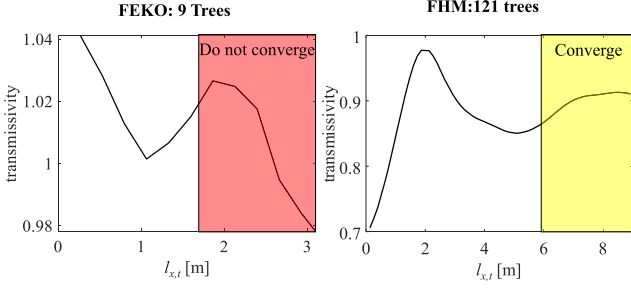


Fig. 9. Convergence comparison between 9 trees and 121 trees.

any trees. As a result, the transmissivity of nine trees is greater than that of actual forest. Additionally, as shown in Fig. 9, simulations with fewer trees do not converge due to edge effects. In contrast, a domain with 121 trees achieves convergence of the transmissivity with respect to $l_{x,t}$. Therefore, this indicates that for the simulation of wave propagation through forested areas, domain with 121 trees and a height of 16 m is sufficiently accurate.

III. P-BAND SIGNAL ANALYSIS ON FOREST

In the previous section, the number of trees is determined, and the scattering model of the FHM is validated. This section illustrates the analysis of *P*-band signal for various forest parameters. The dielectric constant of trees on forest varies seasonally. The dielectric constant is expected to be the highest during summer and the lowest during winter due to its relation with moisture and temperature [3]. Considering a minimum dielectric constant of 3 representative of winter conditions and a maximum dielectric constant of 20 representative of summer conditions for a variety of trees [3], the *P*-band signal simulations span all seasons. In the wave scattering model, the angles of the incident waves are the same with the previous section.

A. 16 m of Tree Height With Trunk of 5 cm Radius

Using 121 trees with a height of 16 m as shown in Fig. 7, the transmissivity for various dielectric constants is analyzed. From the forest wave scattering model, total electric fields and total magnetic fields on the ground plane beneath trees (at $z = 0$ m) are illustrated in Fig. 10. We can observe high amplitudes (sometimes greater than 1) of *P*-band signals between trees along the x -direction due to the fact that the signals between trees are less attenuated and the incident waves passing through trees and reflected waves by other trees could be coherent. Fig. 11(a) shows the convergence of the transmissivity computation. Following the completion of the convergence block, the transmissivity versus dielectric constant is shown in Fig. 11(b). Since higher dielectric constants of trees lead to higher scattering coefficients and loss, an increase in the dielectric constant decreases the transmitted power. Over the entire range of dielectric constant, *P*-band can penetrate forest with a transmissivity of about 0.7 (summer) or greater than 0.9 (winter).

To indicate the impact of dielectric constant on the spatial variation of transmission fields, the complex correlation coefficient is computed within the computation block in Fig. 4. High

correlation means that the spatial distribution of propagated *P*-band signals is less sensitive to the variation of dielectric constants. The correlation coefficient is derived from the electric fields by using complex-valued samples [19]. Because of the oscillatory nature of the real and imaginary values of electric field components on the bottom plane, the mean electric field is significantly smaller than the sample values in the correlation coefficient. This leads to the following equation:

$$\widehat{C}_{er,jk} \approx \frac{\sum_{i=1}^{N_{px}N_{py}} \bar{E}_{er,j}(x_i, y_i) \cdot \bar{E}_{er,k}^*(x_i, y_i)}{\sqrt{\sum_{i=1}^{N_{px}N_{py}} |\bar{E}_{er,j}(x_i, y_i)|^2 \sum_{i=1}^{N_{px}N_{py}} |\bar{E}_{er,k}(x_i, y_i)|^2}}, \quad j \neq k \quad (10)$$

where indices j and k indicate the dielectric constant for comparison and the reference dielectric constant, respectively, and a summation index i indicates the i th segment as shown in Fig. 12. We carry out a numerical integration over discretized segments on the bottom plane underneath trees, thus the segments Δx and Δy should be less than a wavelength. We divide the bottom plane with a segment length of 0.067 m, about 1/12th of one λ .

To ensure convergence, the procedure described in Fig. 4 is performed. Without loss of generality, we let the reference dielectric constant be 6. The tolerance for convergence criteria is 0.06. Applying (10) to the computation block, a convergence is achieved after $l_{x,t} = 6$ m, as shown in Fig. 13(a). As a result, the correlation coefficients for the 121-tree case are illustrated in Fig. 13(b). The amplitude of the correlation coefficient decreases as the difference between the reference dielectric constant and the other dielectric constants grows, and the phase of the correlation coefficients remains in the range of -4° to 6° . As the dielectric constant difference increases, the spatial variation of *P*-band signals increases. Although the amplitude and phase of transmitted fields vary with dielectric constants, they are highly correlated up to dielectric constant of 20 with the correlation coefficient amplitude above 0.88 and phase change of less than 6° .

B. Dependence on Tree Size

The height and trunk radius of trees can have a large variation. The variation with respect to heights is shown in Fig. 14(a). The scattering model to this case is generated by the FHM. Since the taller tree leads to an increase in scattering, the transmissivity is reduced. As shown in Fig. 14(b), the transmissivity has an approximate linear dependence on the tree height and the dielectric constant has an influence on the slope.

Based on the generated results, we have developed a parametric model for *P*-band signal transmissivities that vary with tree heights (with a fixed trunk diameter of 10 cm). A data set provides the parametric model of different tree heights through curve fitting. As shown in Fig. 14(b), the first-order polynomial fitting, $T \approx ah + 1$, can represent the simulated transmissivity based on the FHM. The polynomial coefficients are shown in Table IV. To validate the parametric model, the transmissivities of $h = 10$ m and $h = 14$ m corresponding to dielectric constant of 3 are obtained by the FHM. As shown in Fig. 14(b), the validation points show good agreement. The correlation coefficient corresponding to this height range is shown in Fig. 15. As the

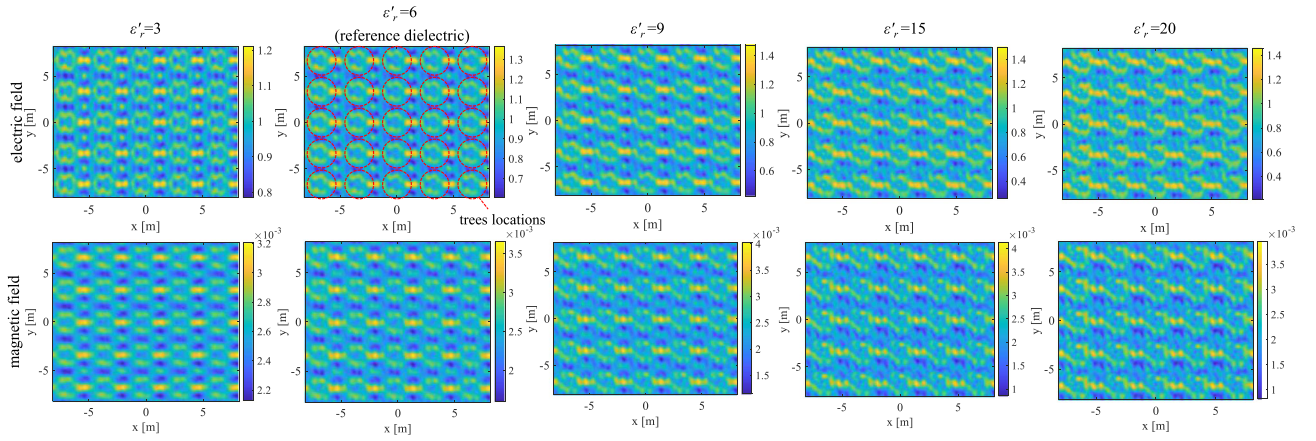


Fig. 10. P-band signals with different dielectric constants on the bottom plane.

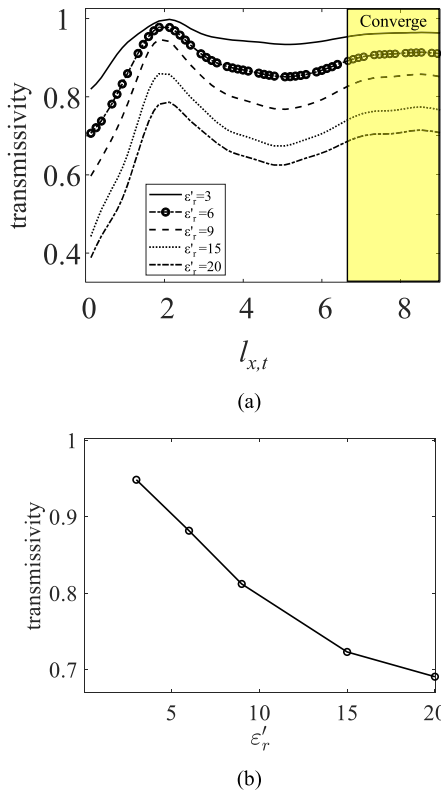


Fig. 11. Transmissivity with different dielectric constants. (a) Convergence of transmissivity. (b) Transmissivity with respect to the complex permittivity.

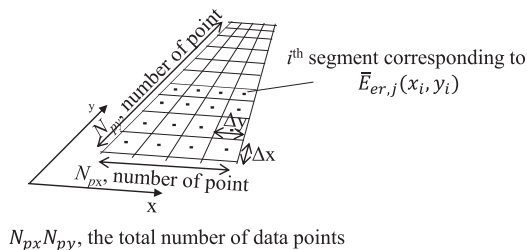


Fig. 12. Segments for calculating correlation function.

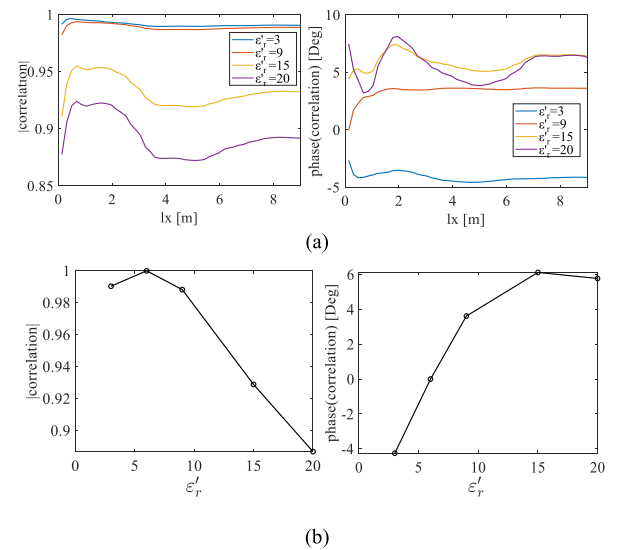


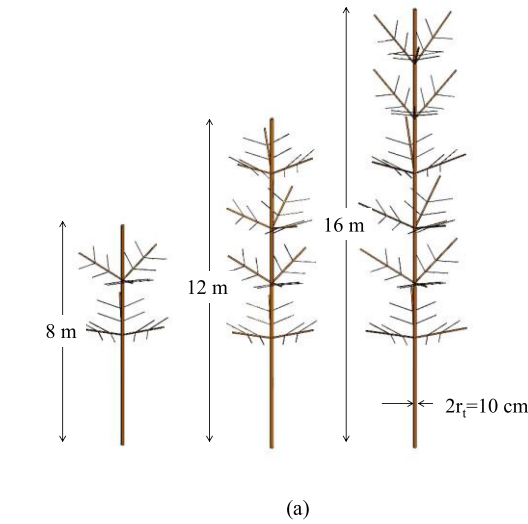
Fig. 13. Correlation of P-band signals with different dielectric constants of trees. Note that the ε'_r means the index j in (10) and the reference dielectric constant k is 6. (a) Convergence of correlation function in amplitude and phase. (b) Convergent correlation value with respect to dielectric constants.

TABLE IV
COEFFICIENTS OF POLYNOMIAL FOR TRANSMISSIVITY: TREE HEIGHT

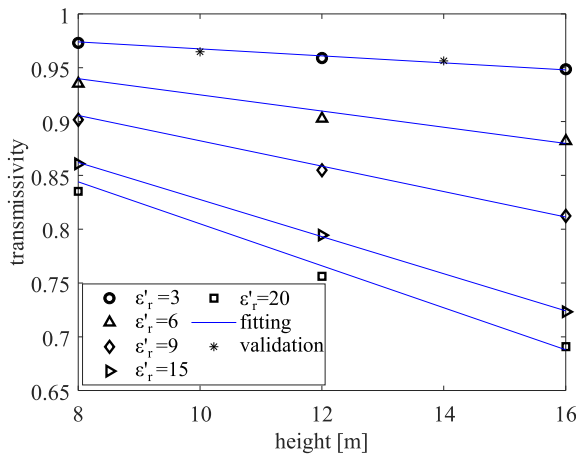
ε_r	3	6	9	15	20
a	$-3.05\text{E-}3$	$-6.66\text{E-}3$	$-1.12\text{E-}2$	$-1.72\text{E-}2$	$-1.81\text{E-}2$

tree height decreases, the correlation between transmission fields for different dielectric constant increases. In the case of a height of 8 m, they are highly correlated with correlation coefficient amplitudes mostly above 0.9 and the phase change of under 2° .

P-band signal modeling for variations in trunk radii was performed. Trees in the model have a fixed height of 16 m, with trunk radii varying between 5 and 15 cm, as illustrated in Fig. 16(a). Since the volume increases with the square of radius, the transmissivity is not linear as shown in Fig. 16(b). As a



(a)



(b)

Fig. 14. Parametric modeling of transmissivity with different tree heights. (a) Geometry of trees. (b) Transmissivity with respect to heights.

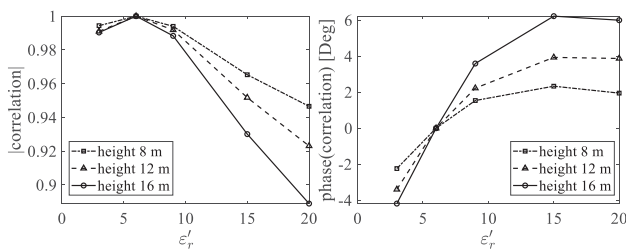
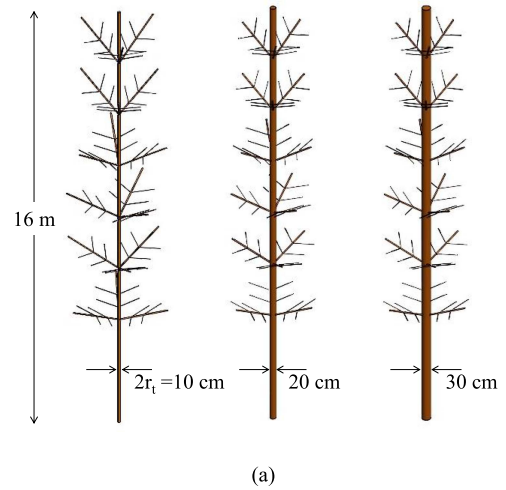
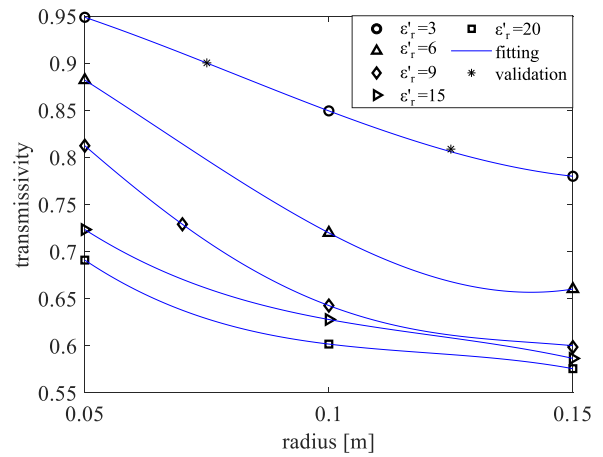


Fig. 15. Correlation coefficients versus tree heights.

result, the parametric model is generated by using curve fitting up to the fourth order as $T = a_3 r_t^4 + a_2 r_t^3 + a_1 r_t + 1$. The coefficients of the polynomial are shown in Table V. The validation points of the parametric model show good agreement with the FHM, as shown in Fig. 16(b). The correlation coefficient corresponding to the trunk radii is shown in Fig. 17.



(a)



(b)

Fig. 16. Empirical modeling of transmissivity with varying trunk radii. (a) Geometry of trees. (b) Transmissivity with respect to radii.

 TABLE V
 COEFFICIENTS OF POLYNOMIAL FOR TRANSMISSIVITY: TRUNK RADII

ϵ_r	3	6	9	15	20
a_1	-2.433E-2	-0.940	-1.588	-8.193	-9.426
a_2	-25.24	-38.18	-77.56	61.64	75.34
a_3	104.1	195.6	792.8	-169.3	-209.1
a_4	0	0	-2.158E3	0	0

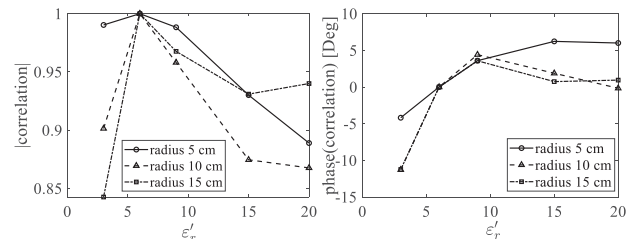


Fig. 17. Correlation coefficients versus tree radii.

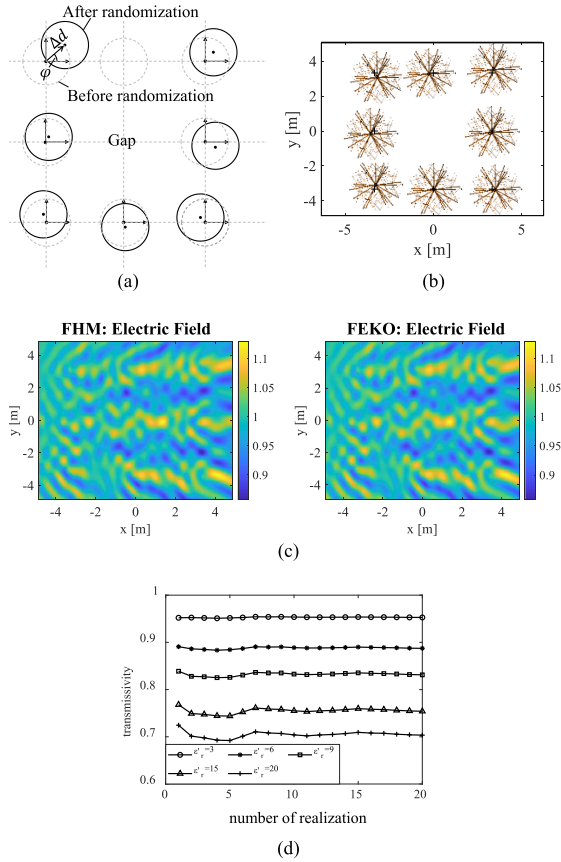


Fig. 18. Study of random locations of 16-m-tall trees. (a) Definition of random variables. (b) Geometric configuration of randomly positioned trees used for validation. (c) Spatial distribution of electric fields obtained by the FHM and FEKO. (d) Transmissivity computation with Monte Carlo simulations of randomized trees.

C. Randomization of Trees (Locations and Different Trees)

To assess the impact of randomly located trees, we perform the FHM for nonperiodic structures [10]. The FHM is suitable for scattering by trees in random positions as the 2-D translation through 2-D SMCG [11] is applied to nonperiodic located trees to speedily translate to periodic grids. Tree locations are randomized by the displacement Δd , the azimuth rotation φ on grid points, and random gaps as shown in Fig. 18(a). Fig. 18(b) shows the validation case of eight trees with a gap. The FHM is applied to this geometric configuration. In Fig. 18(c), the results show that the electric fields of random locations of trees are identical between the FHM and FEKO. Following that, the FHM is extended to a forest of 112 trees with dimensions of $35.8 \times 35.8 \text{ m}^2$. By performing Monte Carlo simulations that average transmissivities over realizations [9], the transmissivities corresponding to dielectric constants are obtained as shown in Fig. 18(d). The difference of transmissivity between trees located on periodic grids and random grids is within 4.3%.

To account for the presence of mixed trees, we conduct a separate study that includes two different tree heights in one forest stand: those 16 and 8 m tall. To validate this study, mixed eight trees are randomly located as shown in Fig. 19(a). The FHM results are in good agreement with that of FEKO, as shown

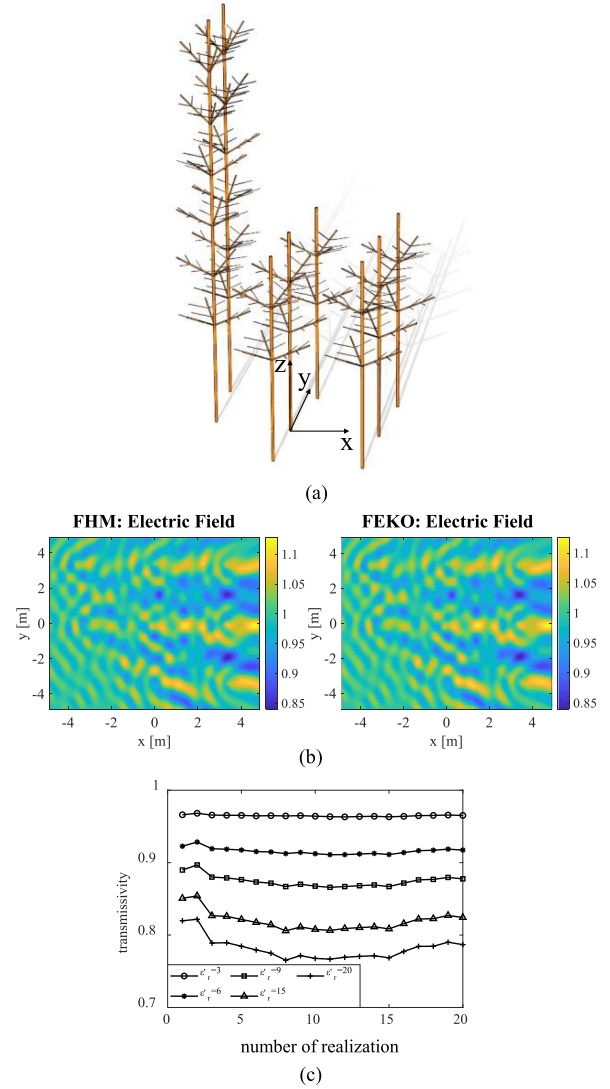


Fig. 19. Investigation of mixed trees with 16 and 8 m tree heights in a forested area. (a) Trees of two different heights and randomized locations for validation. (b) Electric fields on the bottom plane corresponding to mixed eight trees by the FHM (left) and FEKO (right). (c) Transmissivity computation of mixed 112 trees with Monte Carlo simulations (trees randomly positioned).

in Fig. 19(b). Using Monte Carlo simulations, we obtain the transmissivities for a forest of 112 trees comprising two different trees. The results are shown in Fig. 19(c).

We compare the transmissivities obtained from the random positions and mixed trees with those obtained from the original positions, using previously obtained results, as shown in Fig. 20(a). For the scenario of the mixed trees, the heights of the trees are randomly selected between 8 and 16 m. As a result, the average ratio of 16 m height trees to the total trees is obtained as 0.47 over all realizations. Our analysis reveals that randomly generated tree positions lead to clustering effects and thus produced higher transmissivity values than nonrandom trees. Furthermore, due to the greater penetration of radio signals through 8-m trees compared to 16-m trees, the mixed trees yield higher transmissivity values than the other two scenarios. The transmissivity of the mixed trees is approximately midway between that of the randomized 16-m trees and the randomized

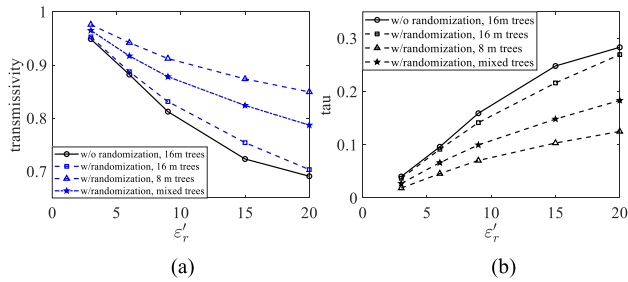


Fig. 20. Comparison of (a) transmissivity and (b) optical thickness among 8 and 16 m randomly positioned trees, randomly positioned 16-m trees, and nonrandom 16-m trees.

TABLE VI
L-BAND [9] AND P-BAND COMPARISON: 8-M TREE

	L-band	P-band
incident plane wave	vertical polarization	
transmissivity	0.58	0.80

8-m trees because the number of 16-m trees used in the mixed tree scenarios is lower than that of 8-m trees.

In order to calculate the optical depth using the FHM, we utilize the relationship between effective transmissivity and optical thickness as follows [8]:

$$\tau_{\text{eff}} = -\cos \theta_i \ln t \quad (11)$$

where t and τ_{eff} are the transmissivity and the effective optical thickness, respectively. This allows us to extract the values of the effective optical thickness, which fits into the RTE model, as shown in Fig. 20(b).

D. L- and P-Band Comparison

The P-band can better penetrate tree canopies due to a longer wavelength than other bands. To analyze its advantage, we compare L-band and P-band transmissivity. For the pair comparison, using the same incident waves, the dielectric constant, and tree sizes as in [9], with a tree height of 8 m and a trunk radius of 12.5 cm, we obtain the P-band transmissivity through the FHM with randomized trees and compare to that of [9]. The results, shown in Table VI, indicate that the transmissivity of P-band is 0.22 higher than the L-band transmissivity. Considering the thick trunks used in the simulation, this supports the notion that P-band radio signals provide better penetration through the forest canopy.

IV. CONCLUSION

In this article, the analysis of the P-band signal propagation through forest has been performed by the FHM. A hypothetical forest consisting of 121 coniferous trees for the domain area, 35.8 m \times 35.8 m, is considered necessary for accurate wave scattering modeling. Therefore, considering the CPU time and memory requirement of scattering simulations, the FHM is used for efficient and fast solutions. To validate the accuracy

of the FHM, the wave scattering model for nine trees is validated by FEKO. To cover seasonal variations, transmissivity simulations with respect to a range of dielectric constant have been performed. Across a range of dielectric constants, it was shown that for P-band forest consisting of a tree height of 16 m transmissivities are higher than 0.69. The winter and the summer conditions show transmissivity values of 0.97 and 0.69, respectively. Using the transmissivity results from a range of dielectric constants, heights, and trunk radii, we have developed a parametric model, which provides the estimated transmissivity based on geometric parameters and dielectric constants of trees. Over seasonal variations in forest with a height of 16-m trees and the radius of 5 cm, the P-band radio signal remains well-correlated (correlation amplitude > 0.89) with relatively small phase variations less than 4° . Furthermore, the FHM is implemented to account for both the randomly positioned trees and the mixed trees, covering various scenarios of the forest. The FHM results show that P-band provides higher penetration through the forest of trees than L-band. Presently we are developing T-matrices that include leaves. At P-band, an approximate calculation gives τ (leaves) of roughly 0.02. Thus, scattering waves are dominated by tree trunks, primary and secondary branches. The proposed analysis will be extended to study radio signal propagation through forest across multiple frequencies, including L-, S-, and C-bands. Electromagnetic modeling for scenarios involving intercepted snow in the canopy requires further research due to the transmissivity variation caused by it.

REFERENCES

- [1] S. Yueh et al., "A P-band signals of opportunity synthetic aperture radar concept for remote sensing of terrestrial snow," in *Proc. IEEE Int. Geosci. Remote Sens. Symp.*, Kuala Lumpur, Malaysia, 2022, pp. 4244–4247.
- [2] S. H. Yueh, R. Shah, X. Xu, B. Stiles, and X. Bosch-Lluis, "A satellite synthetic aperture radar concept using P-band signals of opportunity," *IEEE J. Sel. Topics Appl. Earth Observ. Remote Sens.*, vol. 14, pp. 2796–2816, Feb. 2021.
- [3] A. Mavrović et al., "Dielectric characterization of vegetation at L band using an open-ended coaxial probe," *Geosci. Instrum., Methods Data Syst.*, vol. 7, no. 3, pp. 195–208, Jul. 2018.
- [4] L. Tsang, M. C. Kubacsí, and J. A. Kong, "Radiative transfer theory for active remote sensing of a layer of small ellipsoidal scatterers," *Radio Sci.*, vol. 16, no. 3, pp. 321–329, May 1981.
- [5] R. H. Lang and J. S. Sighu, "Electromagnetic backscattering from a layer of vegetation: A discrete approach," *IEEE Trans. Geosci. Remote Sens.*, vol. GRS-21, no. 1, pp. 62–71, Jan. 1983.
- [6] S. A. Torricco, C. Utku, and R. H. Lang, "UHF propagation through a trunk dominated forest," *Radio Sci.*, vol. 55, no. 7, pp. 1–17, Jul. 2020.
- [7] CST Studio Suite, Dassault Systemes. [Online]. Available: <https://www.3ds.com/products-services/simulia/products/cst-studio-suite/>
- [8] H. Huang, L. Tsang, A. Colliander, and S. H. Yueh, "Propagation of waves in randomly distributed cylinders using three-dimensional vector cylindrical wave expansions in Foldy–Lax equations," *IEEE J. Multiscale Multiphys. Comput. Techn.*, vol. 4, pp. 214–226, 2019.
- [9] W. Gu, L. Tsang, A. Colliander, and S. H. Yueh, "Hybrid method for full-wave simulations of forests at L-band," *IEEE Access*, vol. 10, pp. 105898–105909, 2022.
- [10] J. Jeong, L. Tsang, W. Gu, A. Colliander, and S. H. Yueh, "Wave propagation in vegetation field by combining fast multiple scattering theory and numerical electromagnetics in a hybrid method," *IEEE Trans. Antennas Propag.*, vol. 71, no. 4, pp. 3598–3610, Apr. 2023.
- [11] C. H. Chan and L. Tsang, "A sparse-matrix canonical-grid method for scattering by many scatterers," *Microw. Opt. Technol. Lett.*, vol. 8, pp. 114–118, 1995.

- [12] L. Tsang, T. H. Liao, R. Gao, H. Xu, W. Gu, and J. Zhu, "Theory of microwave remote sensing of vegetation effects, SoOp and rough soil surface backscattering," *Remote Sens.*, vol. 14, no. 15, Jul. 2022, Art. no. 3640.
- [13] Altair Feko, Altair Engineering, Inc. [Online]. Available: www.altairhyperworks.com/feko
- [14] F. Ulaby and M. El-Rayes, "Microwave dielectric spectrum of vegetation—Part II: Dual-dispersion model," *IEEE Trans. Geosci. Remote Sens.*, vol. GRS-25, no. 5, pp. 550–557, Sep. 1987.
- [15] S. Tan, J. Zhu, L. Tsang, and S. V. Nghiem, "Microwave signatures of snow cover using numerical Maxwell equations based on discrete dipole approximation in bicontinuous media and half-space dyadic Green's function," *IEEE J. Sel. Topics Appl. Earth Observ. Remote Sens.*, vol. 10, no. 11, pp. 4686–4702, Nov. 2017.
- [16] W. Lee and D. Jiao, "Fast structure-aware direct time-domain finite-element solver for the analysis of large-scale on-chip circuits," *IEEE Trans. Compon., Packag. Manuf. Technol.*, vol. 5, no. 10, pp. 1477–1487, Oct. 2015.
- [17] W. Gu, L. Tsang, A. Colliander, and S. H. Yueh, "Multifrequency full-wave simulations of vegetation using a hybrid method," *IEEE Trans. Microw. Theory Techn.*, vol. 70, no. 1, pp. 275–285, Jan. 2022.
- [18] L. Tsang, J. A. Kong, K.-H. Ding, and C. O. Ao, *Scattering of Electromagnetic Waves, Theory and Applications*, vol. 1. New York, NY, USA: Wiley, 2001.
- [19] G. B. Arfken and H. J. Weber, *Mathematical Methods for Physicists*, 7th ed. Burlington, MA, USA: Elsevier, 2012.
- [20] F. T. Ulaby, K. Sarabandi, K. McDonald, M. Whitt, and M. C. Dobson, "Michigan microwave canopy scattering model," *Int. J. Remote Sens.*, vol. 11, no. 7, pp. 1223–1253, 1990.



Jongwoo Jeong (Graduate Student Member, IEEE) received the B.S. degree in electronic engineering from the Kumoh National Institute of Technology, Gumi, South Korea, in 2013, and the M.S. degree in electrical and computer engineering from the Ulsan National Institute of Science and Technology, Ulsan, South Korea, in 2015. He is currently working toward the Ph.D. degree with the Department of Electrical Engineering and Computer Science, University of Michigan, Ann Arbor, MI, USA.

From 2015 to 2021, he was with the CTO Division, LG Electronics Company Ltd., Seoul, South Korea, where he was involved in the development of IC packaging, magnetic actuator, and acoustic waves. His research interests include wave propagation, multiple scattering theory, computational electromagnetics, and signal/power integrity.

Mr. Jeong was a recipient of the Fulbright Scholarship for graduate study in 2021.



Leung Tsang (Life Fellow, IEEE) was born and completed High School in Hong Kong. He received the B.S., M.S., and Ph.D. degrees from the Massachusetts Institute of Technology, Cambridge, MA, USA.

From 1983 to 2014, he was with the University of Washington, where he was the Chair of the EE Department from 2006 to 2011. From 2001 to 2004, he was on leave at the EE Department, City University of Hong Kong. Since January 2015, he has been a Professor with the Department of EECS, University of Michigan, Ann Arbor, MI, USA. He is the lead

author of four books: *Theory of Microwave Remote Sensing and Scattering of Electromagnetic Waves* (volumes 1–3). His research interests include remote sensing, random media and rough surfaces, computational electromagnetics, electromagnetic compatibility, and photonic crystals.

Dr. Tsang was the Editor-in-Chief for the IEEE TRANSACTIONS ON GEOSCIENCE AND REMOTE SENSING from 1996 to 2000 and was the President of the IEEE Geoscience and Remote Sensing Society (GRSS) from 2006 to 2007. He is an honorary life member of GRSS. He has been the Chair of PIERS and the President of Electromagnetics Academy since 2008. He was the recipient of the Distinguished Achievement Award from GRSS in 2008. He was also the recipient of the Golden Florin Award in 2010, the William Pecora Award cosponsored by USGS and NASA in 2012, the IEEE Electromagnetics Award in 2013, and the van de Hulst Light Scattering Award in 2018. He is a Fellow of the Optical Society of America and a member of the U.S. National Academy of Engineering.



Xiaolan Xu (Member, IEEE) received the B.Eng. degree from Zhejiang University, Hangzhou, China, in 2006, and the M.S. and Ph.D. degrees in electrical engineering from the University of Washington, Seattle, WA, USA, in 2008 and 2011, respectively.

In 2012, she joined the Jet Propulsion Laboratory, California Institute of Technology, Pasadena, CA, USA, as a Postdoctoral Research Associate and later became a Scientist in 2014. Her expertise lies in the field of applied electromagnetics, electromagnetic wave propagation, and scattering properties from snow-covered terrain, vegetated land surface, and bare soil. She specialized in the development of forward modeling and retrieval algorithm with applications to earth remote sensing from space.

Dr. Xu was the recipient of the URSI Santimay Basu Award in 2020.



Simon H. Yueh (Fellow, IEEE) received the Ph.D. degree in electrical engineering from the Massachusetts Institute of Technology, Cambridge, MA, USA, in January 1991.

From February to August 1991, he was a Postdoctoral Research Associate with the Massachusetts Institute of Technology. In September 1991, he joined the Radar Science and Engineering Section with the Jet Propulsion Laboratory (JPL), California Institute of Technology, Pasadena, CA, USA. He was the Supervisor of Radar System Engineering and Algorithm

Development Group from 2002 to 2007, the Deputy Manager of Climate, Oceans and Solid Earth section from 2007 to 2009, and the Section Manager from 2009 to 2013. He was the Project Scientist of the National Aeronautics and Space Administration (NASA) Aquarius mission from January 2012 to September 2013, the Deputy Project Scientist of NASA Soil Moisture Active Passive Mission from January 2013 to September 2013, and has been the SMAP Project Scientist since October 2013. He has been the Principal/Co-Investigator of numerous NASA and DOD research projects on remote sensing of ocean salinity, ocean wind, terrestrial snow, and soil moisture. He has authored four book chapters and authored/coauthored more than 300 publications and presentations.

Dr. Yueh was the recipient of the 2021 IEEE J-STARS Prize Paper Award, 2014 IEEE GRSS Transaction Prize Paper Award, 2010 IEEE GRSS Transaction Prize Paper Award, 2002 IEEE GRSS Transaction Prize Paper Award, the 2000 Best Paper Award in the IEEE International Geoscience and Remote Sensing Symposium 2000, and the 1995 IEEE GRSS Transaction Prize Paper Award for a paper on polarimetric radiometry. He was the recipient of the JPL Lew Allen Award in 1998, Ed Stone Award in 2003, NASA Exceptional Technology Achievement Award in 2014, and NASA Outstanding Public Leadership Medal in 2017. He was an Associate Editor for *Radio Science* from 2002 to 2006 and the Editor-in-Chief for IEEE TRANSACTIONS ON GEOSCIENCE AND REMOTE SENSING from 2018 to 2022. He is a member of URSI Commission-F.



Steven A. Margulis received the B.S. degree in civil and environmental engineering from the University of Southern California, Los Angeles, CA, USA, in 1996, and the M.S. and Ph.D. degrees in civil and environmental engineering from the Massachusetts Institute of Technology, Cambridge, MA, USA, in 1998 and 2002, respectively.

He is currently a Professor with the Department of Civil and Environmental Engineering, University of California, Los Angeles, CA, USA.